Theory of *L*-Star Combustion Instability with Temperature Oscillations

J. S. T'IEN,* W. A. SIRIGNANO,† AND M. SUMMERFIELD‡
Princeton University, Princeton, N.J.

Low-frequency nonacoustic instability of solid-propellant rocket motors is being investigated by adopting a combustion model which allows the flame temperature to oscillate with the chamber pressure. Two different chamber gasdynamic situations are analyzed; in one the chamber gases are without dissipation and mixing and in the other they are well-stirred which eliminates entropy waves. The neutral stability lines are found to depend on the propellant and steady-state parameters and the nondimensional gas residence time in the chamber. Comparison with the results under isothermal conditions shows that the temperature oscillations have a destabilizing effect, especially when the nondimensional gas residence time is small. When the nondimensional gas residence time is large, the stability boundaries approach the boundary of intrinsic instability of the burning rate. Comparison of experimental data with theoretical predictions has been made. Its results indicate that the qualitative aspects of the model are correct, the quantitative predictions are sufficiently close that a more critical comparison is needed. And this, in turn, requires more precise measured data of the propellant surface temperature and the surface activation energy.

Nomenclature

A_c = cross-sectional area of combustion chamber, cm²
A_t = nozzle throat area, cm²
C_D = nozzle discharge coefficient
E_s = surface activation energy, kcal/mole
F_1 = chamber transfer function
F_2 = combustion transfer function
$F_s, \hat{F}_s$ = system transfer function
F_s^* = system transfer function—well-stirred case
H = $Q_s/c_p(\bar{T}_s - T_0)$, nondimensional surface heat release parameter
l = length of the chamber, measured from propellant surface, cm
m = surface pyrolysis exponent
n = steady state burning pressure exponent
p = pressure, lb/in.²
P = $p/\bar{p}$, nondimensional pressure
Q_s = surface heat release, see Eq. (10), cal/g
r = burning rate, cm/sec
R = $r/\bar{r}$ nondimensional burning rate
s = Laplace transform time
S = nondimensional entropy, see Ref. 7
t = time, sec
T = temperature, °K
x = distance, measured from propellant surface, cm
X = $x/(\alpha/\bar{r})$, nondimensional distance
$\bar{u}$ = mean velocity of gas in the chamber, cm/sec
α = thermal diffusivity, cm²/sec
γ = ratio of specific heats
δ = $(l/\bar{u})/(\alpha/\bar{r}^2)$, nondimensional gas residence time in the chamber or the ratio of gas residence time in the chamber to the solid-thermal-relaxation time
θ = $(T - T_0)/(\bar{T}_s - T_0)$, nondimensional temperature, see Ref. 7
ξ = $(\bar{T}_s - T_0)/\bar{T}_f$
ρ = density, g/cm³
τ = $t/(\alpha/\bar{r}^2)$, nondimensional time
ω = nondimensional frequency of oscillation, rad.

Subscript

f = flame
g = gas
p = propellant
s = propellant surface
0 = cold end of the propellant

Superscript

$\bar{(\ )}$ = steady state
$(\ )'$ = perturbation
$\sim$ = Laplace transformed variable

Presented as Paper 68-179 at the AIAA 6th Aerospace Sciences Meeting, New York, January 22–24, 1968; received November 15, 1968; revision received July 7, 1969. Based on work performed under Contract AF49 (638) 1405 issued by the Propulsion Division, Air Force Office of Scientific Research.

* Assistant-in-Research, Guggenheim Laboratories, Department of Aerospace and Mechanical Sciences. Student Member AIAA.

† Associate Professor of Aerospace and Mechanical Sciences. Associate Fellow AIAA.

‡ Professor of Aerospace Propulsion. Fellow AIAA.

I. Introduction

LOW-FREQUENCY, nonacoustic instability in the solid-propellant rocket motor has been found in practice for many years, in which either chuffing or sinusoidal pressure oscillations can appear. Several theories[1–5] have been developed trying to explain the phenomena and their analyses are based upon a closed-loop system consisting of the pressure and burning rate response functions. A closed-loop relation is needed because a pressure perturbation affects the burning rate through the combustion process and the burning rate in turn affects the pressure through the gas flow in the chamber and the nozzle. Thus we see that a complete stability analysis of the rocket motor requires a realistic combustion model and a correct gasdynamic formulation in the chamber flow.

Akiba and Tanno[1] were the first to establish the closed-loop system and investigated the stability of a given propellant and rocket motor. Sehgal and Strand[2] did the same thing. Coates, Cohen, and Harvill[4] applied the Denison and Baum combustion model to their analysis and investigated the trend of stability of propellants and motors. Beckstead et al.[3,5] dealt with the same problem but they did not employ any specific model, instead they used the combustion response function and the combustion time lag as free parameters. More recently, Oberg[12] also coupled the chamber gasdynamics with the Denison and Baum's combustion model and made comparison with the L^* burner data of some pro-

pellants. Oberg[12] and Culick[13] also tried to show that the low frequency nonacoustic oscillation is the lowest mode of the acoustic oscillation. However, this observation is hardly new; it is discussed by Crocco and Cheng in their monograph[8] (see, for example, p. 85).

In all the previous analyses, the temperature in the combustion chamber is assumed to be uniform and constant (except Ref. 12, in which it is assumed that the temperature and pressure are isentropic and uniform). This may be copied from the early works of low-frequency instability analysis of the liquid-propellant rocket motors,[6] in which the combustion model does not give any flame temperature expressions, and the plausible isothermal flame assumption is essential to obtain a result. However, with the advances of solid-propellant combustion models, it is now possible to calculate the flame temperature exactly and this assumption becomes unnecessary. In Ref. 7, it has been shown that the flame temperature is in general oscillating with the pressure and that near-isentropic response exists within the range of low-frequency oscillations. Therefore, in this paper, we avoid any ad hoc assumption regarding the flame temperature, and let it be determined through the proper physical process. More specifically, the combustion model established in Ref. 7 is applied to two different gasdynamic situations in the end-burning rocket chamber; in one the dissipation and mixing of chamber gases are neglected and in the other the gases are well-stirred.

II. Case 1: Nondissipative and Nonmixing Chamber Gases

In this case, we consider the one-dimensional end-burning rocket motors. Only pressure coupled instability is considered here. The coordinate system has its origin moving with the propellant surface, so that the chamber length or volume is a function of time. When the frequency of the oscillating pressure is low and the chamber is not too large, the pressure in the chamber can be considered uniform, so $p = p(t)$ replaces the momentum equation. Under the assumption that the dissipation and mixing in the chamber are neglected, the energy equation can be replaced by the isentropic relationship for a fixed particle. That is

$$\frac{T(x,t)}{T(0,t - x/\bar{u})} = \left[\frac{p(t)}{p(t - x/\bar{u})}\right]^{(\gamma-1)/\gamma} \tag{1}$$

We further assume that the flame is thin compared to the length of the chamber, so that $x = 0$ denotes the position of the flame and $T(0,t - x/\bar{u})$ is the flame temperature at time $t - x/\bar{u}$. In this case an entropy or temperature wave can be developed as a consequence of the entropy generated in the flame and the isentropic relation of a fixed particle in the chamber.

The only governing equation left is the mass conservation equation, which can be written as

$$\rho_p A r = \dot{m}_e + A_c \frac{d}{dt}\int_0^{l(t)} \rho_g(x,t)dx \tag{2}$$

where $\dot{m}_e$ is the mass flux through the nozzle.

If the subsonic portion of the supercritical nozzle is short the flow can be considered to be in the quasi-steady state. When the nozzle is long, the quasi-steady-state approximation will introduce some error. It has been shown that a lead component exists in the nozzle transfer function which is proportional to the frequencies.[9] The present analysis can be modified to this situation without fundamental difficulties. Cheng[10] has shown that the long nozzle effect is to increase the gas residence time in the analysis. We expect the same thing here. So, taking a short nozzle,

$$\dot{m}_e = C_D A_t p(t)/[T(l,t)]^{1/2} \tag{3}$$

The last term of (2) can be written as

$$A_c \frac{d}{dt}\int_0^{l(t)} \rho_g(x,t)dx = A_c \int_0^{l(t)} \frac{\partial \rho_g(x,t)}{\partial t} dx + \rho_g(l,t)A_c r \tag{4}$$

Neglecting $\rho_g A_c r$ compared with $\rho_p A_c r$, (2), (3), and (4) give

$$\rho_p A_c r = \frac{C_D A_t p(t)}{[T(l,t)]^{1/2}} + A_c \int_0^l \frac{\partial \rho_g(x,t)}{\partial t} dx \tag{5}$$

If we substitute (1) and the equation of state for a perfect gas into (5), we can express (5) in terms of burning rate, pressure and flame temperature (i.e., T at $x = 0$). For the convenience of utilizing the results for the flame temperature expression,[7] we nondimensionalize all of the variables in the following way:

$$\begin{aligned} X &= x/(\alpha/\bar{r}),\ \tau = t/(\alpha/\bar{r}^2),\ R = r/\bar{r} \\ P &= p/\bar{p},\ \theta = (T - T_0)/(\bar{T}_s - T_0) \end{aligned} \tag{6}$$

Substituting (1), (6), and the equation of state into (5), and considering small unsteady perturbation, we obtain

$$R'(\tau) = \frac{3\gamma - 1}{2\gamma} P'(\tau) - \frac{\gamma - 1}{2\gamma} P'(\tau - \delta) + \frac{1}{\gamma}\delta \frac{dP'(\tau)}{d\tau} - \xi\theta_f'(\tau) + \frac{1}{2}\xi\theta'_f(\tau - \delta) \tag{7}$$

where $\delta = (l/\bar{u})/(\alpha/\bar{r}^2)$ is the nondimensional gas residence time in the chamber and $\xi = (\bar{T}_s - T_0)/\bar{T}_f$ is a steady-state parameter. In obtaining Eq. (7), we note that the integral term in Eq. (5), when substituted by the equation of state and Eq. (1), produces three parts, i.e.,

$$\int_0^l \frac{dP'(\tau)}{d\tau} dx,\ \int_0^l \frac{dP'(\tau - x\bar{r}^2/\alpha\bar{u})}{d\tau} dx$$

$$\int_0^l \frac{d\theta'_f(\tau - x\bar{r}^2/\alpha\bar{u})}{d\tau} dx$$

The last two terms when integrated become $P'(\tau - \delta)$ and $\theta'_f(\tau - \delta)$, respectively, and the first term yields $\delta dP'(\tau)/d\tau$.

The flame temperature perturbation θ'_f in Eq. 7 is connected to the pressure and burning rate perturbations through the consideration of the combustion model. Therefore, here we will describe briefly the combustion model which yields the combustion burning rate response which is required to complete the chamber coupling problem.

The combustion model established in Ref. 7 describes the low-to-moderate frequency oscillations of a composite solid propellant. The gas phase equations are treated in a quasi-steady manner, and by assuming proper flame structure the heat flux to the solid surface is determined. With this heat flux from the gas phase given, the unsteady equation of the solid phase can be solved for small oscillatory perturbations of pressure. If only the exponential type solution is of interest, the response of the burning rate perturbation to a pressure perturbation is given by the combustion transfer function $F_2(s)$:

$$F_2(s) = \frac{\tilde{R}'(s)}{\tilde{P}'(s)} = \frac{2mBs}{m + s(2A - 1) - (m + s)(1 + 4s)^{1/2}} \tag{8}$$

where

$$\begin{aligned} A &= (2H - 1)m \\ B &= (2H - 2 - m^{-1})n \end{aligned}$$

The important parameters of the solid propellant are the nondimensional surface heat release parameter H, the surface pyrolysis exponent m and the steady-state burning pressure index n. H is defined by

$$H = Q_s/c_p(\bar{T}_s - T_0) \tag{9}$$

Table 1 Comparison of theory and experimental data

Propellant	U-TF	A-35	A-91	A-97	
Composition	75% AP 18% PBAA 5% Al 2% Cu	75% AP 25% PU	67% AP 25% PU 8% Al	66.5% AP 25% PU 8% Al 0.5% Cu	Ref. 5
$\bar{r}$, in./sec at 100 psia	0.310	0.133	0.108	0.150	Ref. 5
n	0.46	0.49	0.52	0.53	Ref. 5
Q_s cal/g	142.3	131.2	105.9	102.9	calculated from Eq. (10)
$\bar{T}_s$, °K	950	860	845	875	
H	0.663	0.710	0.590	0.542	calculated from Eq. (9)
m	6.50	6.82	6.80	6.76	calculated from Eq. (11)
Theoretically calculated critical δ	0.14	0.33	0.14	0.07	
Theoretically calculated critical ω	2.5	2.0	2.4	2.8	
Experimental critical δ	0.08–0.16	0.14–0.33	0.13–0.22	0.05–0.14	Ref. 5
Experimental critical ω	2.7–3.9	2.2–3.5	3.0–3.4	3.4–5.7	Ref. 5

Where Q_s is the dimensional surface heat release. To evaluate Q_s we first subdivide the surface heat release into an endothermic decomposition occurring right at the solid surface, followed by an exothermic ammonia/perchloric acid gas-phase flame occurring so close to the surface (with respect to the O/F flame) that it is effectively collapsed and, being so very thin, its entire heat release is conducted back into the solid.[14,15] The gaseous fuel acts only as a diluent in this very rapid reaction. The exothermicity of the A/PA flame is sufficient to make the over-all process at the surface appear exothermic. The extent of the exothermicity increases with the AP content of propellant. More specifically, the Q_s is expressed by the approximate formula[14,15]

$$Q_s(\text{cal/g}) = \%AP \times 250 - \%\ \text{Fuel} \times 225 - \%\ \text{Al(or Cu)} \times 67 \quad (10)$$

With Q_s given by Eq. (10), H is estimated to be between 0.5 and 0.75 for most composite propellants. Calculated values of H for several practical propellants are listed on Table 1 for the purpose of experimental comparison. The surface pyrolysis exponent m is largely a measure of the surface activation energy. For linear analysis it is expressed by

$$m = (E_s/\mathcal{R}\bar{T}_s)(1 - T_0/\bar{T}_s) \quad (11)$$

The steady-state burning pressure index n can be experimentally measured. Therefore theoretically all the propellant parameters can either be calculated from its composition or obtained by proper measurements. Practically, however, the surface temperature of the propellant is difficult to measure and the surface activation energy is also somewhat uncertain. The effects of this difficulty on the result of theoretical prediction will be discussed in the section on experimental comparisons.

Considering the energy balance across the flame, the flame temperature perturbation can be expressed as a linear combination of pressure and burning rate perturbations[7]

$$\theta'_f = c_1 P' + c_2 R' \quad (12)$$

where

$$c_1 = (2H - 2 - m^{-1})n,\ c_2 = (2 + m^{-1} - 2H)$$

Substituting (12) into (7), a functional relationship between pressure and burning rate is obtained

$$(1 + \xi c_2)R'(\tau) - \tfrac{1}{2}\xi c_2 R'(\tau - \delta) = \frac{1}{\gamma}\delta\frac{dP'(\tau)}{d\tau} + \left(\frac{3\gamma - 1}{2\gamma} - \xi c_1\right)P'(\tau) + \left(\frac{1 - \gamma}{2\gamma} + \frac{1}{2}\xi c_1\right)P'(\tau - \delta) \quad (13)$$

Taking the Laplace transform of (13) with respect to τ and denoting the transformed time by s, we obtain

$$F_1(s) = \tilde{P}'(s)/\tilde{R}'(s) = (k_1 + k_2 e^{-\delta s})/(k_3 + \frac{1}{\gamma}\delta s + k_4 e^{-\delta s}) \quad (14)$$

where

$$k_1 = 1 + \xi c_2,\ k_3 = (3\gamma - 1)/2\gamma - \xi c_1$$

$$k_2 = -\tfrac{1}{2}\xi c_2,\ k_4 = (1 - \gamma)/2\gamma + \tfrac{1}{2}\xi c_1$$

All of the k's are functions of propellant and steady-state parameters (H, m, n, and ξ). $F_1(s)$ is the chamber transfer function which is a measure of the pressure response to the burning rate perturbation.

Following Akiba and Tanno,[1] we form a closed-loop system and the stability of the rocket motor is then determined by a study of the system transfer function. Two ways of formulating the system transfer function are possible:

$$F_s(s) = \tilde{P}'(s)/\tilde{R}'(s) = F_1(s)/[1 - F_1(s)F_2(s)] \quad (15)$$

$$\hat{F}_s(s) = \tilde{R}'(s)/\tilde{P}'(s) = F_2(s)/[1 - F_1(s)F_2(s)] \quad (16)$$

In (15), the burning rate perturbation is taken as an input and the pressure perturbation as an output and in (16), vice versa. Later it will be shown that these two system transfer functions result in the same stability criterion, which then expresses explicitly that in a nonacoustic unstable rocket motor, the amplifying of pressure oscillation is accompanied by the amplifying of the burning rate and vice versa. For a given propellant and rocket motor, the stability can be determined by using the Satche diagram.[8] However, if the trend or a stability map is desired, we prefer the following method. Putting $s = \lambda + i\omega$ and $\lambda = 0$, the neutral stability line is determined by the poles of $F_s(i\omega)$ or $\hat{F}_s(i\omega)$, which from (15) or (16) occur at

$$1 - F_1(i\omega)F_2(i\omega) = 0 \quad (17)$$

Thus, we see immediately that $F_s(s)$ and $\hat{F}_s(s)$ give the same stability criterion. Equation (17) is a complex function of H, m, n, ξ, δ, and ω. We can separate it into two real equations, and, in principle, we can eliminate ω to obtain a functional relationship between H, m, n, ξ, and δ for the stability boundaries. However, this elimination process is difficult due to the complicated form of (17). Instead ω is used as a running variable to plot the boundary lines. In this way, (17) is reduced to two real equations. One is an algebraic expression for H in term of all the other parameters, the other is a third degree algebraic equation in m with n, ξ, δ, and ω as coefficients. So with various sets of these coeffi-

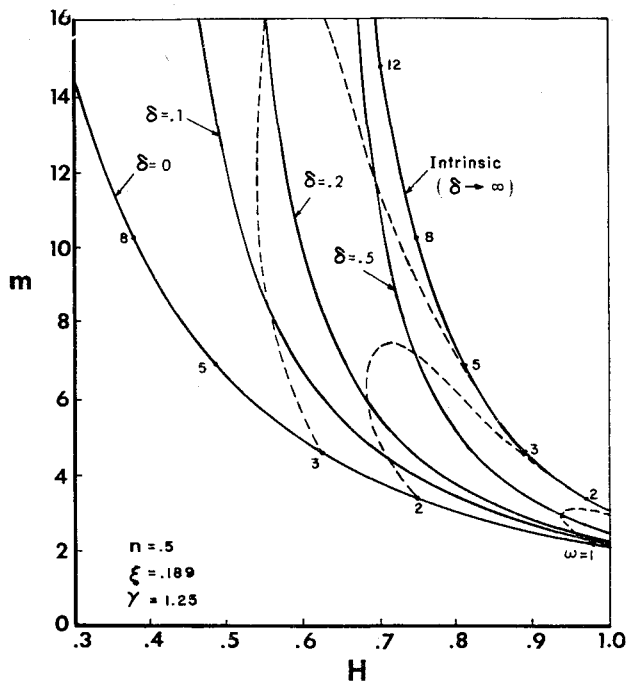

Fig. 1 Stability map: nondissipative and nonmixing chamber gases.

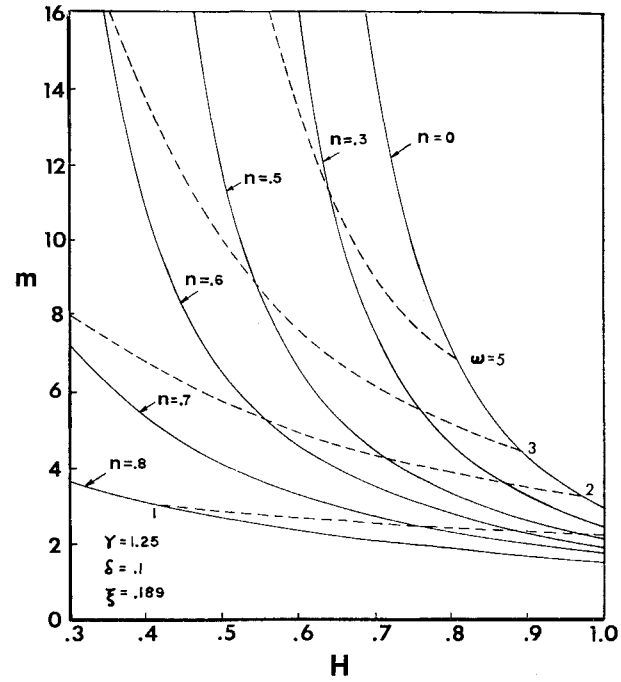

Fig. 2 Influence of n on a stability map.

cients given, m and H can be solved exactly for the neutral stability lines.

Figure 1 is an example of a stability map. The boundary lines are plotted for different values of the nondimensional gas residence time δ. As with the previous treatment,[1-5] it is found that small δ is more unstable. Since δ must be positive the $\delta = 0$ line is the limit on whose left side the propellant is unconditionally stable.§ The other limit occurs when $\delta \to \infty$, and in this case, it approaches the boundary of the intrinsic instability of the burning rate. This can be seen very easily from (14) and (15). When $\delta \to \infty$, $F_1(i\omega) \to 0$, and the stability criterion $F_3(i\omega) \to \infty$ reduces to $F_2(i\omega) \to \infty$, which is the criterion for the intrinsic instability of the burning rate. The distribution of stability boundaries for different δ values can be explained as follows. When δ is equal to zero, the pressure feedback from the chamber is in phase with the burning rate, so a relatively small burning rate response is enough to produce instability. As δ increases, the pressure feedback tends to be out of phase with the burning rate and its magnitude decreases. A larger combustion burning rate response is needed for instability and this shifts the stability boundary toward the intrinsic unstable line.

We observe from Fig. 1 that most of the unstable region has a quite small critical gas residence time δ and in general it is less than the period of oscillation $2\pi/\omega$. Therefore, although existence of entropy waves is allowed in the chamber, these waves do not exist for most propellants in a nonacoustic unstable motor. Instead, the temperature in the chamber oscillates with time in a more or less uniform (space-wise) fashion.¶ Only when the propellant is sufficiently close to the intrinsic boundary, are entropy waves possible. The frequencies distribution in Fig. 1 may also be interesting. If we follow a constant m line starting from $\delta = 0$ then as H and δ increase, ω decreases first until a minimum value is reached and then increases back to its original value at the $\delta \to \infty$ line.

Figure 1 is plotted with the parameters n and ξ constant. It is natural then to ask what are their influences on the stability boundaries. Figure 2 is plotted for different values of n for the case $\delta = 0.1$. Larger values of n are found to be destabilizing, and the boundary lines are very sensitive to the change of n. For $n = 0.8$, for example, almost all of the exothermic AP composite propellants are unstable for $\delta = 0.1$. For $n = 0$, the stability boundary again shifts to the intrinsic boundary. The reason is simple, for $n = 0$, there will be no burning rate response to pressure perturbations and so the motor can be unstable only when the burning rate is intrinsically unstable. In the combustion model, the steady-

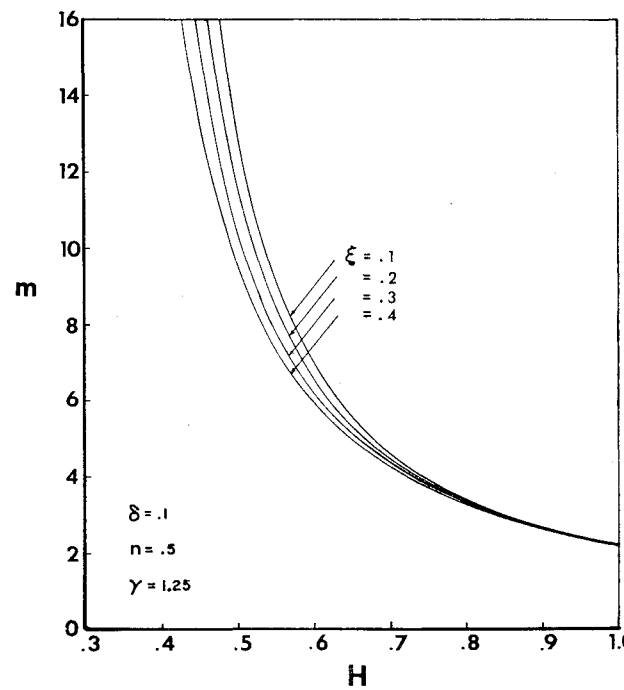

Fig. 3 Influence of ξ on a stability map.

§ Actually, the $\delta = 0$ line has predicted a somewhat larger unstable domain for the practical rocket motors. Since practically no motor can have zero gas residence time, even with a chamber fully loaded with propellant, the subsonic portion of the nozzle contributes finite δ value; this effect, however, has been neglected in the present analysis.

¶ In Ref. 5, the authors assume a small δ to period ratio and claim constant temperature in the chamber. Actually, this assumption only assures a uniform temperature distribution, not a constant one with time.

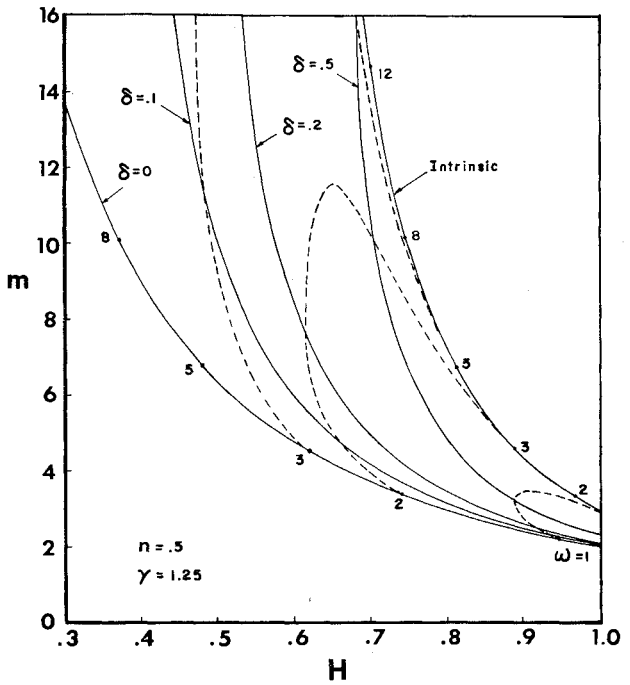

Fig. 4 Stability map: well-stirred chamber.

state burning rate and pressure relation is $\bar{r} = a\bar{p}^n$. Actual AP composite propellant data show that the $\bar{r} - \bar{p}$ curve is not exactly a straight line but somewhat curved in a logarithmic plot. It is therefore essential to fit the n value for each different steady-state pressure used (we are allowed to do this, because in a small perturbation analysis, the pressure will not change much from the mean value). Although n is only very weakly dependent on p, the stability boundaries are quite sensitive to small n changes.

The influence of the steady-state parameter ξ is seen in Fig. 3. The fractional flame temperature perturbation $T'_f/\bar{T}_f$ is equal to $\xi\theta'_f$ so a large value of ξ means a large flame temperature oscillation and is shown to be more unstable. Since $\xi = (\bar{T}_s - T_0)/\bar{T}_f$, we see that an increase of the steady-state flame temperature has a stabilizing effect. The influences of the steady-state surface temperature and the propellant conditioning temperature is more complicated because of the way in which the parameter H is defined, $H = Q_s/c_p(\bar{T}_s - T_0)$ and the probable dependence of m on $\bar{T}_s$. An increase of $\bar{T}_s - T_0$ increases ξ but, on the other hand, decreases H. If we neglect the influence of $\bar{T}_s$ on m, then a considerable increase of $\bar{T}_s - T_0$ only increases ξ by a small amount with no change in m, and as seen from Fig. 3, this only shifts the boundary a little. On the other hand, H will decrease by an appreciable amount, so that an increase of $\bar{T}_s - T_0$ is more likely to be stabilizing.

III. Case 2: Well-Stirred Combustion Chamber

In the previous section, the gases in the combustion chamber are assumed to be without dissipation, so that entropy or temperature waves are allowed to exist. However, when there is a turbulent motion in the chamber, entropy gradients tend to decrease so that the entropy or temperature waves will be suppressed. Therefore, the case of the well-stirred chamber has been studied to model this situation. However, as seen from the results of the previous section, the most unstable cases occur when the gas residence time is so small that the entropy wavelength is considerably longer than the chamber length. Therefore, while the entropy oscillates with time, there is little spacewise variation when δ is small. Without large gradients, little dissipation would occur, and the well-stirred model should not apply. Instead the first model should apply.

The temperature, pressure and entropy relation in the chamber can be written as

$$T'(x,t)/\bar{T}_f = [(\gamma - 1)/\gamma]P'(t) + [(\gamma - 1)/\gamma]S'(x,t) \quad (18)$$

when the chamber is unstirred, and

$$S'(x,t) = \bar{S}e^{i\omega(t-x/\bar{u})}$$

If the situation is such that there could be an entropy wave existing in the chamber for the unstirred case, then for the well-stirred case with large δ, we can suppress the entropy term by setting

$$S'(x,t) = 0 \text{ for } 0 < x \leqslant l$$

As a result of this averaging process, the temperature and density in the chamber become uniform; and

$$T'(t)/\bar{T}_f = [(\gamma - 1)/\gamma]\, P'(t) \quad (19)$$

Substituting (19) into the mass conservation Eq. (5), we obtain the chamber transfer function:

$$F_1^*(s) = 1\Big/\left(\frac{\gamma + 1}{2\gamma} + \frac{\delta}{\gamma}s\right) \quad (20)$$

Substituting (20) and (8) into (17), the neutral stability lines can be calculated as shown in Fig. 4. The stability map looks similar to that of the unstirred case, but predicts a little larger unstable domain for small δ. However, for the reason we just mentioned, these results are not reliable in that limit. Only when δ reaches the order of $2\pi/\omega$, the results begin to become valid. And seen from Fig. 4, this is possible only when the values of the propellant parameters are very close to the intrinsic boundary line.

IV. Comparison of the Different Treatments of the Chamber Gasdynamics

In Refs. 1–5, the same low-frequency nonacoustic instability problem was treated using various combustion models. However, all the treatments assume constant temperature in the chamber. It is therefore worthwhile to discuss and

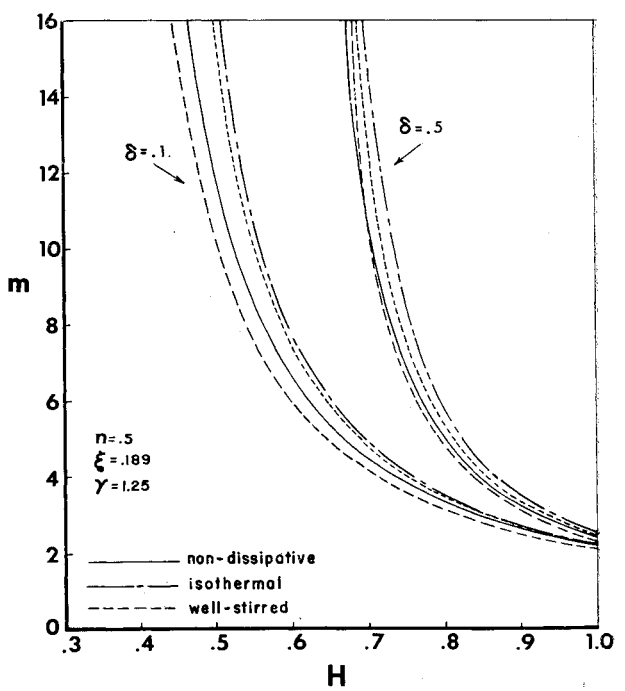

Fig. 5 Comparison of stability domains with different treatment of chamber gasdynamics.

compare the results when the temperature is allowed to vary. In Refs. 1 and 2, the combustion models imply that the flame temperature is a constant. So one may think that under the assumptions of short gas residence time and isothermal flame temperature, the temperature in the chamber can be treated as a constant. However, it has been shown in Refs. 7 and 11, that the flame is in general not isothermal and that any ad hoc assumption regarding the flame temperature will violate the energy balance across the flame. In Ref. 4, the Denison and Baum model[11] was used. In that model, the flame temperature is given by an explicit expression which in general will oscillate with the pressure, so treatment of the chamber temperature as a constant is inconsistent with the combustion model. Also, when the gas residence time becomes large, entropy and temperature waves may appear. Perhaps the best argument for the isothermal treatment is that the temperature oscillations have only a negligible effect on the stability boundaries. However, this conjecture has never been proven. Here, using the same combustion model, a calculation based on the constant chamber temperature condition has been performed to serve as a comparison with the results of the previous sections. Two sets of boundary lines are plotted in Fig. 5 corresponding to the cases of δ equal to 0.1 and 0.5. Only the nondissipative and the isothermal boundaries are compared. We see that the temperature oscillations have a destabilizing effect, especially when δ is small. From Table 1, we find that for many practical propellants δ is around 0.1 or 0.2, which is indeed quite small. Therefore, this finite difference between the two boundary lines can become important if the rocket motor is operating near the stability boundaries. The deviation from isothermal boundaries is actually due to two effects; the flame temperature oscillations and the temperature nonuniformity in the chamber. When δ is very small, the former effect dominates; the latter effect becomes considerable only when δ is large enough to allow a considerable temperature nonuniformity in the chamber. In Fig. 5, we have plotted a small dotted line which is obtained by assuming constant flame temperature but allowing chamber temperature to vary with pressure isentropically. So the difference of this line with the nondissipative boundary is the contribution of flame temperature oscillation and the difference with the isothermal line is the contribution of temperature waves. The weighting of the aforementioned two effects is clearly illustrated in Fig. 5 by the relative position of the small dotted lines between the nondissipative and isothermal boundaries for the cases of $\delta = 0.1$ and $\delta = 0.5$

V. Comparison of Theory and Experiment

Since the analysis of nonacoustic oscillation is relatively simple and the L^* burner is relatively easy to fabricate, a comparison of the results of nonacoustic analysis with the L^* burner data can serve as a good test for the combustion model used in the analysis. In the following we are going to compare our theoretical predictions to the data[5] of four propellants; Utah-TF, JPL A-35, A-91, and A-97. The quantities we are going to compare are the critical (at the neutral stability limit) gas residence time and the critical oscillating frequency. Since the experimental data is very scattered, we list their ranges on Table 1. Next we try to estimate the propellant parameters H, m, and n based on the composition of propellants and other measured information and calculate the theoretical δ and ω. Then we compare them with the experimentally determined quantities.

The following numerical values were used in the theoretical calculations: $c_p = 0.33$ cal/g°K, $T_0 = 300$°K, $E_s = 18$ kcal/mole. $\bar{T}_s$ for U-TF propellant is estimated to be 950°K, then assuming the pre-exponential factor and the surface activation energy are the same for all four propellants, we calculate the $\bar{T}_s$ for the other three propellants based on their experimental burning rate.** Next we calculate Q_s from (10), H from (9) and m from (11). With all these propellant parameters found we can calculate δ and ω from Eqs. (17, 8, and 14); their values are listed on Table 1. We see from Table 1 that the theoretical predicated δ falls within the range of experimental values for all four propellants. But all the theoretical ω are somewhat lower than the experimental values although they are very close. This discrepancy, however, does not discredit our combustion model since the value of H and m, hence δ and ω, are quite sensitive to the choice of $\bar{T}_s$ and E_s whose values are uncertain. Although we believe we have picked their values reasonably, a slight change could produce a more favorable comparison. Take for example, the A-35 propellants. If we use $\bar{T}_s$ equal to 900°K instead of 860°K, we get $H = 0.645$ instead of .71, $m = 6.67$ instead of 6.82 and $\delta = 0.18$, $\omega = 2.3$ which are both within the range of experimental data. Take A-97 propellant, for another example; if we take $\bar{T}_s = 950$°K instead of 875°K, $E_s = 22$ kcal/g instead of 18 kcal/g then $H = 0.48$, $m = 8.0$ which give $\delta = 0.06$, $\omega = 3.45$. Both of them now are within the experimental range. Since the values of these parameters we are adjusting here are within our uncertainty of knowledge (e.g., Beckstead and Price[5] use $\bar{T}_s = 750$°–1100°K, $E_s = 22$ kcal/g and 30 kcal/g, while Steinz[14] and Merkle[15] use $E_s = 16$ kcal/g), a more critical quantitative comparison is hindered by the sensitivity of δ and ω to these parameters. A more precise measurement or some other method of comparison is needed. Despite the fact the quantitative aspect is not entirely conclusive, the qualitative picture is correct as seen from the table. The theory predicts A-97 is most stable, U-TF and A-91 come next and A-35 last. The experimental data show the same trend. The same is true for the ordering of frequencies. Therefore, the destablizing effect of large surface heat release is experimentally supported (provided their n's are approximately equal, for example, the larger H and lower n of U-TF has the same value of theoretical δ as that of A-91 which has a lower H and higher n).

Three of the propellants we compared here contain aluminum. Although there exist several theories on the role of aluminum powder on combustion instability, such as particulate damping and thermal inertia effect,[16] we did not specifically consider them here. We would just mention that by the addition of aluminum to the propellant (at the expense of AP or fuel or both), the value of surface heat release parameter H is changed [see Eq. (10)]. Therefore, aside from those specific effects previously mentioned, the simple "H effect" on instability could shift the rocket motor from one side of the stability line to the other.

In conclusion, from the comparison of theory and experiment, we feel that the qualitative picture of the combustion model is correct; the quantitative prediction is sufficiently close that a more critical comparison is needed. This, however, requires a more precise measurement of the values of surface temperature of the propellants and their surface activation energy.

References

[1] Akiba, R. and Tanno, M., "Low Frequency Instability in Solid Rocket Motors," *Proceedings of the First International Symposium on Rockets and Astronautics*, 1959, Tokyo, Japan, pp. 74–82.

[2] Sehgal, R. and Strand, L. D., "A Theory of Low-Frequency Combustion Instability in Solid Rocket Motors," *AIAA Journal*, Vol. 2, No. 4, April 1964, pp. 696–703.

[3] Beckstead, M. W., Ryan, N. W., and Baer, A. D., "Nonacoustic Instability of Composite Propellant Combustion," *AIAA Journal*, Vol. 4, No. 9, Sept. 1966, pp. 1622–1628.

** As indicated in Ref. 5, for the three JPL propellants we used here, the dimensional gas residence time is not strictly proportional to $\bar{r}^2$. Here we have chosen to evaluate all the relevant quantities at 100 psia.

[4] Coates, R. L., Cohen, N. S., and Harvill, L. R., "An Interpretation of L^* Combustion Instability in Terms of Acoustic Instability Theory," *AIAA Journal*, Vol. 5, No. 6, June 1967, pp. 1097–1102.

[5] Beckstead, M. W. and Price, E. W., "Nonacoustic Combustor Instability," *AIAA Journal*, Vol. 5, No. 11, Nov. 1967, pp. 1989–1996.

[6] Crocco, L., "Aspects of Combustion Stability in Liquid Propellant Rocket Motors, Part I," *Journal of the American Rocket Society*, Vol. 21, No. 6, Nov. 1951, pp. 163.

[7] Krier, H. et al., "Nonsteady Burning Phenomena of Solid Propellant: Theory and Experiments," *AIAA Journal*, Vol. 6, No. 2, Feb. 1968, pp. 278–285.

[8] Crocco, L. and Cheng, S. I., *Theory of Combustion Instability in Liquid Propellant Rocket Motors*, 1st ed., Macmillan, New York, 1957.

[9] Tsien, H. S., "The Transfer Functions of Rocket Nozzles," *Journal of the American Rocket Society*, Vol. 22, No. 3, May 1952, pp. 1939.

[10] Cheng, S. I., "Low-Frequency Combustion Stability of Liquid Rocket Motor with Different Nozzles," *Jet Propulsion*, Vol. 25, 1955, p. 163.

[11] Denison, R. and Baum, E., "A Simplified Model for Unstable Burning in Solid Propellants," *Journal of the American Rocket Society*, Vol. 31, No. 8, Aug. 1961, p. 1112.

[12] Oberg, C. L., "Combustion Instability: The Relationship between Acoustic and Nonacoustic Instability," *AIAA Journal*, Vol. 6, No. 2, Feb. 1968, pp. 265–271.

[13] Culick, F. E. C., "Some Nonacoustic Instabilities in Rocket Chamber Are Acoustic," *AIAA Journal*, Vol. 6, No. 7, July 1968, pp. 1421–1423.

[14] Steinze, J. A. and Summerfield, M., "Mechanism of Burning of Composite Solid Propellants With Special Reference to Low Pressure Combustion Phenomena," *Advances in Chemistry Series*, American Chemistry Society, 1969, to be published.

[15] Merkle, C. L., Turk, S. L., and Summerfield, M., "Extinguishment of Solid Propellants by Depressurization: Effects of Propellant Parameters," AIAA Paper 69-176, New York, 1969.

[16] Summerfield, M. and Krier, H., "Role of Aluminum in Suppressing Instability in Solid Propellant Rocket Motors," *Problems of Hydrodynamics and Continuum Mechanics*, English ed., Society for Industrial and Applied Mathematics, Philadelphia, Pa., 1969.